Soil Dynamics and Earthquake Engineering 177 (2024) 108427

Contents lists available at ScienceDirect

Soil Dynamics and Earthquake Engineering

journal homepage: www.elsevier.com/locate/soildyn

Artificial neural network-based prediction model of elastic floor response spectra incorporating dynamic primary-secondary structure interaction

Madhavi Latha Annamdasu [a], S.P. Challagulla [a,b,*], Denise-Penelope N. Kontoni [c,d,**], J. Rex [e], Mohammed Jameel [f], Felipe Vicencio [g]

[a] Department of Civil Engineering, Koneru Lakshmaiah Education Foundation, Vaddeswaram, Guntur, Andhra Pradesh, 522302, India
[b] Thornton Tomasetti, Baner, Pune, Maharashtra, 411045, India
[c] Department of Civil Engineering, School of Engineering, University of the Peloponnese, GR-26334, Patras, Greece
[d] School of Science and Technology, Hellenic Open University, GR-26335, Patras, Greece
[e] Department of Civil Engineering, Malla Reddy Engineering College (Autonomous), Secunderabad, Telangana, 500100, India
[f] Department of Civil Engineering, College of Engineering, King Khalid University, Abha, 61421, Saudi Arabia
[g] Facultad de Ingenieria, Arquitectura y Diseño, Universidad San Sebastian, Santiago, Chile

ARTICLE INFO

Keywords:
Primary structure
Secondary structure
Seismic behavior
Floor response spectrum
Tuning ratio
Dynamic interaction
Artificial neural networks

ABSTRACT

The evaluation of the Floor Response Spectrum (FRS) holds paramount significance in assessing the seismic behavior of secondary structures. Precise FRS prediction empowers engineers to make informed decisions concerning structural design, retrofitting, and safety precautions. This study aims to scrutinize the impact of dynamic interaction between primary and secondary structures on FRS. Both the elastic primary structure (PS) and elastic secondary structure (SS) employ a single-degree-of-freedom (SDOF) system. Governing motion equations for both coupled (with dynamic interaction) and uncoupled (without dynamic interaction) systems are formulated and solved numerically. The study investigates how variations in the vibration period of PS (T_p), tuning ratio (T_r), mass ratio (μ), and damping ratio (ξ_s) of SS influence FRS. The FRS impact remains minimal at $\mu = 0.001$ (0.1%); however, with increasing mass ratio, PS-SS dynamic interaction significantly affects SS's spectral acceleration response. Coupled analysis is crucial only for secondary structures tuned to the primary structure's vibration period ($0.8 \leq T_r \leq 1.2$). This study utilizes two-layer feed-forward Artificial Neural Networks (ANNs) for FRS prediction. The Levenberg-Marquardt (LM) backpropagation (BP) algorithm trains the network using a comprehensive dataset. In summary, it is evident that the ANNs, once trained, enable accurate prediction of the FRS, exhibiting a R^2 of 99%. Additionally, a design expression is formulated utilizing the ANN model and subsequently compared with the existing formulation.

1. Introduction

A building structure comprises elements that do not resist any loads. Such building elements generally are called Secondary structures (SSs). These structures are broadly categorized into three groups: architectural components, mechanical and electrical components, and building contents. Depending on the nature of their failure, secondary structures can be categorized as components sensitive to acceleration or those sensitive to displacement. Deformation failure arises from excessive inter-storey building drift, whereas acceleration failure results from either inertial force within the component or rocking/sliding caused by unanchored or marginally anchored conditions. Many seismic codes implemented in earthquake-prone areas aim to predict the maximum acceleration, thereby estimating the resulting maximum inertial force induced by seismic shaking on SSs. Consequently, this study focuses solely on acceleration-sensitive non-structural components or secondary structures due to this limitation. When a structure is subjected to an earthquake ground motion, it can magnify the motion, causing floor accelerations to exceed the peak ground acceleration (PGA). SSs are subjected to these amplified accelerations, resulting in severe damage to secondary structures and their connections to a structure if they are not considered in their design. The survivability of SSs after an earthquake is

* Corresponding author. Thornton Tomasetti, Baner, Pune, Maharashtra, 411045, India.
** Corresponding author. Department of Civil Engineering, School of Engineering, University of the Peloponnese, GR-26334, Patras, Greece.
E-mail addresses: cprakash@thorntontomasetti.com (S.P. Challagulla), kontoni@uop.gr (D.-P.N. Kontoni).

https://doi.org/10.1016/j.soildyn.2023.108427
Received 21 October 2023; Received in revised form 3 December 2023; Accepted 21 December 2023
Available online 30 December 2023

critical for ensuring the continuation of emergency services, ensuring public safety, and minimizing the financial burden of the subsequent damage. Despite their name, secondary structures are far from insignificant. Furthermore, sometimes secondary structures may be costlier than the primary structure (PS) [1,2]. Secondary structures have been shown to be vulnerable to earthquakes in recent decades [3–6]. Several large hospitals were forced to evacuate during the 1994 Northridge earthquake in Los Angeles due to the failure of critical secondary structures such as emergency power systems, medical equipment control systems, and water supply pipe systems [7]. Given the importance of ensuring SS integrity during seismic events, further study is needed to create credible performance-based design criteria for SSs.

The seismic response of the SSs has been studied extensively for many decades for maintaining the safety of the public and for mitigating the financial impact of the resulting damage. A common method to obtain the seismic demand on the secondary structures is the floor response spectrum (FRS) method. The conventional approach for estimating the input load on a secondary structure (SS) connected to a primary structure is through the utilization of the floor response spectrum method [8–10]. Engineers commonly apply this technique to design secondary structures. The underlying presumption of this method is that the secondary structure remains independent of the primary structure, and the presence of the secondary structure doesn't influence the dynamic response of the primary system, and vice versa. However, this assumption may become invalid in cases where the SS holds substantial weight, leading to potential interaction between the primary and secondary structures. In such instances, the consideration of the combined system becomes necessary [11–13]. Disregarding the interaction typically leads to an overestimation of the demand for the secondary structure, consequently causing an excessively cautious design [14]. Therefore, it is required to investigate the seismic behavior of secondary structures with the dynamic interaction between the primary and secondary structures, and to create accurate and practical methods for determining secondary structure seismic response.

Numerous scholars have investigated the interaction effects and dynamic characteristics of the integrated system by employing a combined model that incorporates both the oscillator and the structure [11, 15–18]. However, earlier research did not examine the influence of the dynamic properties of a primary and secondary structure on the seismic performance of a secondary structure. As a result, in this paper, the single-degree-of-freedom (SDOF) elastic primary structure and the SDOF elastic secondary structure are employed to study the dynamic interaction effects between them. The effects of various parameters, such as the fundamental vibration period of the primary structure, mass ratio, and the damping ratio of the secondary structure, on the seismic response of a SS in the form of FRS, are investigated.

Despite its simplicity, constructing the FRS involves multiple calculation steps. Employing a prediction model that accurately encompasses a substantial array of structures could offer practical benefits. Modern advancements in computer hardware and software have paved the way for the utilization of Artificial Neural Networks (ANNs) as computational models capable of addressing various tasks including prediction, classification, data processing, robotics, and engineering challenges [19–25]. Hence, the objective of this research is to assess the effectiveness of utilizing the ANNs as a computational tool for predicting the elastic floor response spectra (FRS). In this study, we present a comprehensive step-by-step procedure for deriving a design expression based on the Artificial Neural Network (ANN) model developed. The primary purpose of this design expression is to assess the FRS. Subsequently, the ANN-based design expression is compared with existing expression available in the current regulations. To further validate the effectiveness of the ANN model, a comparative analysis is conducted. This analysis involves comparing the FRS obtained through the ANN equation with those derived from dynamic time-history analyses for different damping ratios of the SS. It's important to note that these damping ratios were not used in the development of the ANN model. The following are the few advantages of ANN modeling over the statistical linear and non-linear regression (NLR):

- There is no need to make prior assumptions about the functional design expression or its form, unlike the case of NLR.
- The degree of nonlinearity of independent parameters doesn't require pre-assumptions either.
- The flexibility to easily adjust the network architecture for precise modeling and prediction is unrelated to the need for functional approximation.
- The simplicity of formulating a generalized design expression for the selected, highly accurate simulation and prediction.

This study represents a pioneering effort in utilizing machine learning techniques to estimate floor response spectra (FRS) while considering the dynamic interaction between the primary and secondary structures. To the best of the authors' knowledge, this is the first time such techniques have been extensively explored in this particular context. The objective of this innovative approach is to address a notable void in the current literature and offer valuable insights into the estimation of Floor Response Spectra (FRS) when dynamic interactions among structural components are at play. The paper is organized as follows: Section 2 provides a concise overview of the modeling of both the coupled and uncoupled systems. Section 3 discusses the selection of ground motions and provides specific details pertinent to this research. In Section 4, the research findings are presented. Section 5 elucidates the development and validation of the ANN-based prediction model, and the paper concludes in Section 6 with succinct summarizing remarks.

2. Modeling and analysis

In this research, an elastic primary structure (PS) and an elastic secondary structure (SS) are both represented using a single-degree-of-freedom (SDOF) system. This study is limited to examining structural systems that exhibit elastic responses. The consideration of inelastic behavior within the PS or SS falls beyond the scope of this research. The elastic model used for the structure serves as a reference case, simulating the theoretical behavior of structures while overlooking nonlinear effects during dynamic response. In this work, the analysis considering the dynamic interaction is called a coupled analysis. The uncoupled analysis neglects the dynamic interaction between the PS and SS. A few analysis cases were done using the uncoupled method to show the apparent effect of the dynamic interaction between the PS and SS on the seismic response of SS. Fig. 1 shows the SDOF primary structure attached to an acceleration-sensitive SDOF secondary structure.

2.1. Uncoupled analysis

In this type of analysis, the dynamic interaction between the PS and SS (Fig. 1) is neglected. The viscous damping ratio (ξ_p) of the PS is assumed to a 5% in this study. The dynamic response of the primary structure for a given earthquake loading can be computed according to Eq. (1).

$$m_p\ddot{x}_p + c_p\dot{x}_p + k_p x_p = -m_p\ddot{x}_g \tag{1}$$

where m_p, c_p, and k_p are the mass, damping, and stiffness of the primary structure: $c_p = 2m_p\xi_p\omega_p$; the frequency of the provided primary structure is denoted as ω_p. The relative acceleration, velocity, and displacement of the primary structure with respect to the ground are represented as $\ddot{x}_p$, $\dot{x}_p$, and x_p, respectively. The ground motion acceleration is denoted as $\ddot{x}_g$. The sum of $\ddot{x}_p$ and $\ddot{x}_g$ corresponds to the absolute acceleration response of the primary structure. To analyze the secondary structure, the absolute acceleration response of the primary structure is given as an input to the secondary structure, and the response of the SS can be computed according to Eq. (2).

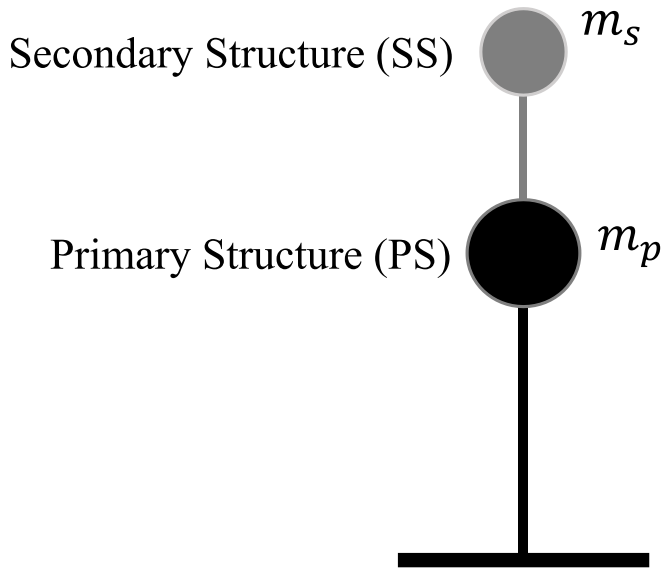

Fig. 1. Primary structure with a Secondary structure.

$$m_s\ddot{x}_s + c_s\dot{x}_s + k_s x_s = -m_s\left(\ddot{x}_p + \ddot{x}_g\right) \tag{2}$$

where m_s, c_s, and k_s are the mass, damping, and stiffness of the SS; $c_s = 2m_s\xi_s\omega_s$; ω_s and ξ_s are the frequency and damping ratio of the given SS; $\ddot{x}_s$, $\dot{x}_s$ and x_s are the relative acceleration, velocity, and displacement of the SS, respectively. The procedure of generating the floor response spectrum without considering the dynamic interaction between the structures is shown in Fig. 2.

2.2. Coupled analysis

Coupled analysis considers the dynamic interaction between the PS and SS. The dynamic response of the primary and secondary structures for a given earthquake loading can be computed according to Eqs. (3) and (4) [26], respectively.

$$m_p\ddot{x}_p + c_p\dot{x}_p - c_s\dot{x}_s + k_p x_p - k_s x_s = -m_p\ddot{x}_g \tag{3}$$

$$m_s\ddot{x}_s + c_s\dot{x}_s + k_s x_s = -m_s\left(\ddot{x}_p + \ddot{x}_g\right) \tag{4}$$

where $\ddot{x}_p$, $\dot{x}_p$, and x_p are the relative acceleration, velocity, and displacement of the primary structure (PS), respectively, with respect to ground; $\ddot{x}_s$, $\dot{x}_s$ and x_s are the relative acceleration, velocity, and displacement of the secondary structure (SS), respectively, with respect to the primary structure. Eqs. (3) and (4) can be written in matrix form as follows:

$$\begin{bmatrix} m_p & 0 \\ 0 & m_s \end{bmatrix}\begin{Bmatrix} \ddot{x}_p \\ \ddot{x}_s \end{Bmatrix} + \begin{bmatrix} c_p & -c_s \\ 0 & c_s \end{bmatrix}\begin{Bmatrix} \dot{x}_p \\ \dot{x}_s \end{Bmatrix} + \begin{bmatrix} k_p & -k_s \\ 0 & k_s \end{bmatrix}\begin{Bmatrix} u_p \\ u_s \end{Bmatrix} = -\begin{Bmatrix} m_p\ddot{x}_g \\ m_s\left(\ddot{x}_p + \ddot{x}_g\right) \end{Bmatrix} \tag{5}$$

The Eqs. (1)–(4) are written as a system of first-order ordinary differential equations and solved numerically using the fourth-order Runge-Kutta technique. The Runge-Kutta method serves as a numerical approach used to estimate solutions to ordinary differential equations (ODEs) given their initial conditions. This method breaks down the problem into smaller increments and computes slopes at multiple points within each increment. Through iterative refinement, it updates the solution at the end of each step, gradually approximating the solution until reaching the intended endpoint. Adjusting the step size allows control over accuracy, where smaller steps yield more precise results. This technique finds extensive application across scientific and engineering domains for solving ODEs, particularly in scenarios where exact analytical solutions are not accessible.

3. Selection and scaling of ground motions

Actual ground-motion data provide a realistic response in the seismic response evaluation technique [27–29]. Such data is freely available in the Pacific Earthquake Engineering Research Centre (PEER) [30] NGA-West2 Database. Consequently, the present investigation involved the analysis of 11 horizontal ground motion excitations corresponding to the hard soil type, following the guidelines outlined in ASCE 7–16 [31]. Ground motions are chosen based on shear wave velocity (V_{S30}) of 360–760 m/s to reflect hard soil, as per National Earthquake Hazard Reduction Program (NEHRP) [32] recommendations. The distance parameter selected for ground motion selection in this study is the

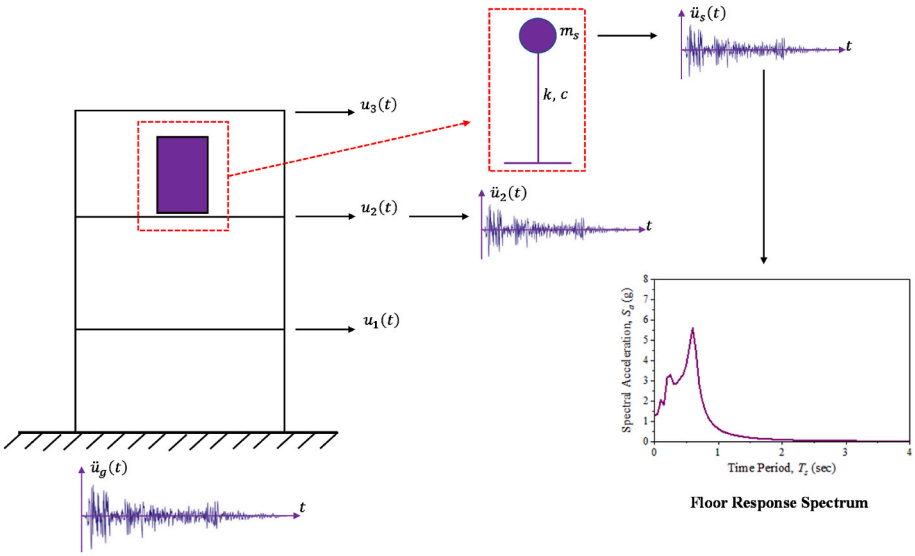

Fig. 2. Procedure for generation of floor response spectrum via uncoupled analysis.

Joyner-Boore distance (R_{jb}), which represents the nearest horizontal distance to the surface projection of the rupture plane. Including a spectrum of R_{jb} distances ranging from 2 to 207 km in this study holds inherent significance in comprehending seismic behavior across diverse distances from the rupture plane. This range of R_{jb} distances offers valuable insights into the characteristics of ground motions at varying proximities to the rupture plane, providing a comprehensive understanding of seismic effects across different distances. Ground motion details are shown in Table 1. This research employs spectrum-compatible ground motions, chosen due to their efficiency in reducing computational workload compared to using numerous ground motions [33]. The generation of earthquake excitations that are spectrum-compatible involves the application of the time-domain spectral matching technique [34]. Fig. 3 illustrates the target spectrum from IS 1893:2016 with 5% damping alongside the mean ground excitation spectra. The average spectrum shall not fall below 90% of the target spectrum for the whole-time range, according to ASCE 7–16. The figure demonstrates that the mean spectra exceed 90% of the target spectra.

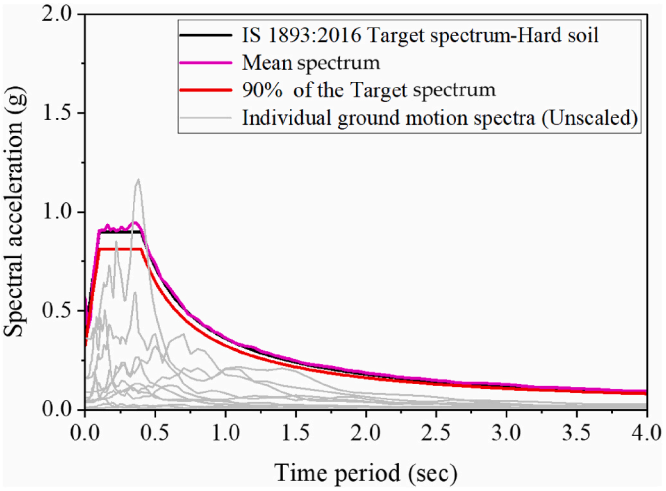

Fig. 3. Target and mean acceleration spectra.

4. Floor response spectrum (FRS)

The determination of the maximum design forces for the secondary structure's design can be achieved through the floor response spectrum (FRS) method [9,35]. However, it's important to note that the FRS method doesn't account for the dynamic interaction between the primary structure (PS) and the secondary structure (SS) [36]. Therefore, the present study attempted to study the FRS by considering the dynamic interaction between the primary and the secondary structure. The floor response spectrum is the spectrum of the secondary structure's peak responses to input ground motion. The effects of the μ (it is defined as the ratio between the mass of the SS and the mass of the PS, i.e., $\mu = m_s/m_p$) and the ξ_s on the floor response spectrum are studied.

Fig. 4 shows the FRS for different damping ratios and mass ratios of the SS for the given damping characteristics of the PS ($T_p = 0.5$ s, $\xi_s = 5\%$). The uncoupled system can be used to estimate the seismic demands on the SS for a tiny mass ratio ($\mu = 0.1\%$), as seen in Fig. 4 for this particular case. The coupled effect of the PS and SS on the FRS is seen when the mass ratio increases for all damping ratios of the SS. The dynamic interaction between the PS and SS shows a significant effect on the magnitude of the spectral acceleration of the SS (Sa_{ss}) at $T_s = 0.5$ s. Such effect is negligible on the behavior of very stiff and flexible secondary structures irrespective of their damping ratio. For the mass ratio of 1%, the peaks of the FRS reduce about 49.2%, 41.8%, 30.4%, and 13.3% at the damping ratios of 0.1%, 0.5%, 2%, and 10%, respectively.

Table 1
Details of ground motions.

Earthquake	Year	Station	M_w	R_{jb} (km)	V_{s30} (m/s)
Helena_ Montana-01	1935	Carroll College	6	2.07	593.35
Helena_ Montana-02	1935	Helena Fed Bldg	6	2.09	551.82
Kern County	1952	Pasadena - CIT Athenaeum	7.36	122.65	415.13
Kern County	1952	Santa Barbara Courthouse	7.36	81.3	514.99
Kern County	1952	Taft Lincoln School	7.36	38.42	385.43
Southern Calif	1952	San Luis Obispo	6	73.35	493.5
Parkfield	1966	Cholame - Shandon Array #12	6.19	17.64	408.93
Parkfield	1966	San Luis Obispo	6.19	63.34	493.5
Parkfield	1966	Temblor pre-1969	6.19	15.96	527.92
Borrego Mtn	1968	Pasadena - CIT Athenaeum	6.63	207.14	415.13
Borrego Mtn	1968	San Onofre - So Cal Edison	6.63	129.11	442.88

From this particular case of analysis, it can be concluded that coupled analysis is required only if the secondary structure is tuned to the vibration period of the primary structure. Otherwise, the uncoupled analysis is sufficient to analyze the seismic behavior of the secondary structure. It can also be deduced that the larger coupling effect on the FRS is observed for the lower damping ratios of the SS.

4.1. Effect of vibration period of the PS on FRS

The effect of the secondary structure's mass ratio and the damping ratio is investigated on the FRS for a given vibration period of the primary structure ($T_p = 0.5$ s) in the previous section. The dynamic characteristics of the primary structure substantially affect the secondary structure's seismic demands [20,37]. As a result, in this section, an attempt has been made to study the effect of a vibration period of the PS on the FRS for a given mass and damping ratio of the SS. The damping ratio of the PS ($\xi_p = 5\%$) is kept constant for all the analysis cases. In this analysis, the tuning ratio (the ratio between the vibration period of the SS, to the fundamental vibration period of the PS) is defined as shown in Eq. (6) to capture the effect of dynamic characteristics of the primary structure.

$$\text{Tuning ratio } (T_r) = T_s \,/\, T_p \tag{6}$$

Fig. 5 shows the variation of the spectral acceleration of a secondary structure with a tuning ratio for different mass and damping ratios of the SS. The FRS for the small mass ratio ($\mu = 0.1\%$) is not shown in this figure since at such a small mass ratio, the coupling effect on the FRS is negligible, as shown in Fig. 4. From Fig. 5, it can be observed that the effect of a dynamic interaction on the FRS is significant in the range of $0.8 \leq T_r \leq 1.2$, while in the range of $T_r < 0.5$ and $T_r > 2$, the insignificant effect of a dynamic interaction on the FRS can be observed for all the considered ξ_s and μ. Hence, it can be concluded that the coupling effect on the FRS can be considered only if the vibration period of the SS is in the vicinity of that of the primary structure. For a given damping ratio, the spectral acceleration of the secondary structure decreases with an increase in the vibration period of the primary structure, irrespective of the mass ratio.

5. Artificial Neural Networks (ANNs)

In recent times, the utilization of machine learning (ML) methods has gained significant traction for predicting diverse outcomes in the realm of structural engineering. In the context of this research, a ML model is utilized to assess the effectiveness of secondary structures and ascertain its potential to establish a meaningful correlation between the provided

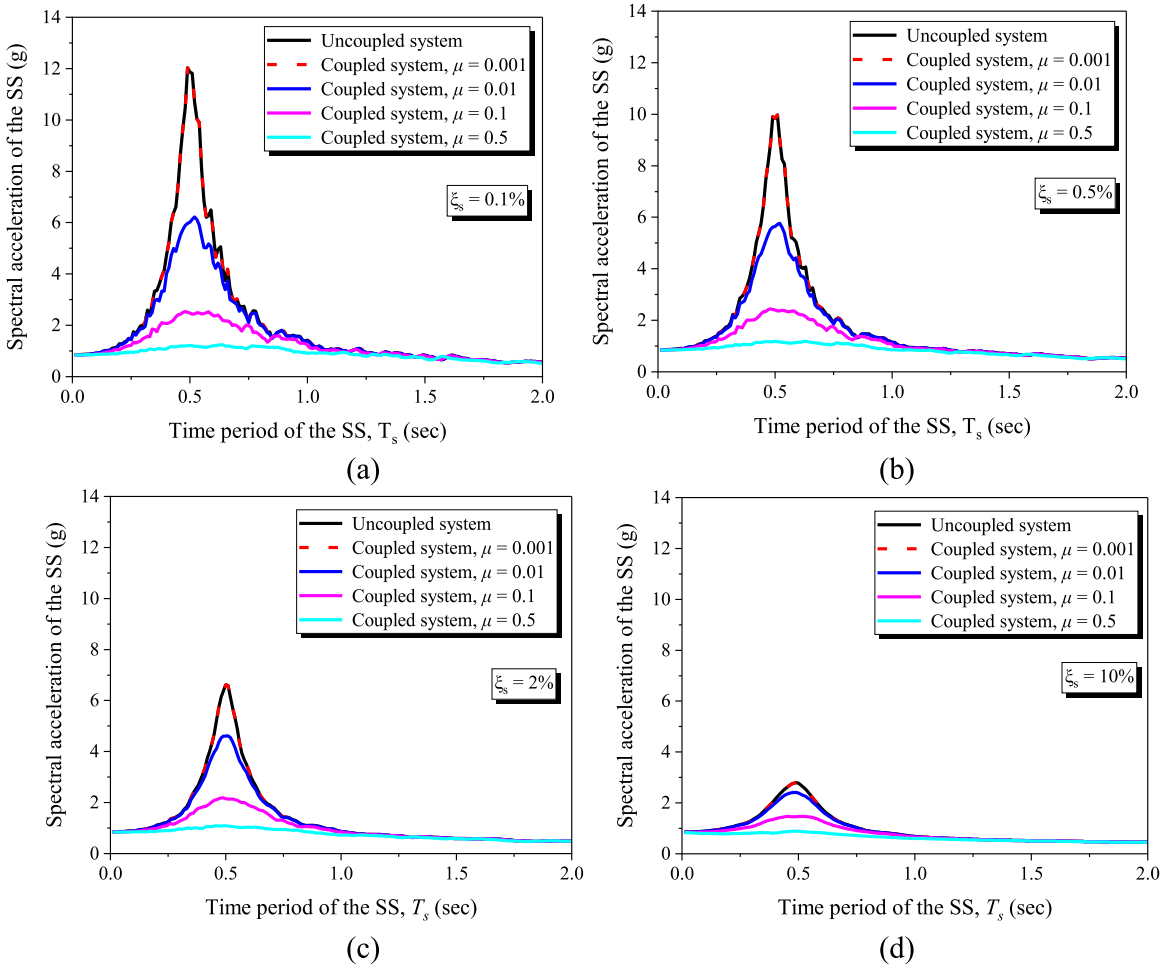

Fig. 4. Effect of mass and damping ratios of the SS on the floor response spectrum for: (a) $\xi_s = 0.1\%$, (b) $\xi_s = 0.5\%$, (c) $\xi_s = 2\%$, and (d) $\xi_s = 10\%$.

inputs and resulting outputs. More specifically, the implementation of an ML technique, the Artificial Neural Network (ANN) model, is undertaken to fulfill this objective. The researchers drew inspiration from the way biological neural networks operate and applied that understanding to create ANN. These ANNs are sophisticated computational models that have demonstrated remarkable capabilities in handling vast amounts of data, tackling complex problems, and navigating uncertain or ambiguous situations. Compared to traditional computational methods, such as mathematical algorithms, neural networks have proven to be more accurate in making predictions and performing calculations [19,38–40]. For the specific task at hand, the researchers focused on predicting a critical parameter called the Floor Response Spectrum (FRS). To achieve this prediction, they employed a specific type of neural network known as a two-layered feed-forward neural network. The two layers in the network are the output layer and the hidden layer. The presence of just a single hidden layer in the neural network is sufficient to achieve accurate approximations of various functions, making the model more efficient and computationally manageable [41]. Fig. 6 illustrates the intricate flowchart that delineates the step-by-step process of predicting FRS through the application of Artificial Neural Networks (ANN).

5.1. Data analysis

The model takes into account various inputs such as the tuning ratio ($T_r = T_s/T_p$), the damping ratio of the SS (ξ_s), the vibration period of the PS (T_p), and the mass ratio (μ). These inputs play a significant role in determining the corresponding FRS, which serves as the ultimate output of the neural network model. The statistical characteristics of the input parameters can be summarized as follows: T_r ranged between 0.1 and 4; ξ_s ranged between 0.1% and 10%; T_p varies between 0.1 and 2 s; and μ varies between 0.001 and 1. Table 2 represents the statistical characteristics of the combined PS-SS model.

Table 3 displays the correlation matrix, which highlights significant relationships among the variables. Particularly noteworthy is the strong negative correlation observed between the vibration period of the primary structure (T_p) and Sa_{ss}, with a correlation coefficient of 0.4565. Additionally, T_r demonstrates a correlation of 0.2217 with Sa_{ss}. On the contrary, both the mass ratio (μ) and damping ratio (ξ_s) exhibit negative correlations with Sa_{ss}. This intricate network of correlations provides valuable insights into the interrelationships among the considered input variables.

5.2. ANN model's architecture

Constructing the ANN model presents a primary challenge in determining the optimal architecture, encompassing factors like hidden layer count, epochs, batch size, and more. While machine learning algorithms learn parameter values—such as node weights and biases—via forward and backpropagation, an additional set of parameters, known as hyperparameters, guide the learning process itself. Tuning these hyperparameters is pivotal to ensure the model effectively tackles the machine learning problem with reliability. In this study, the trial-and-error methodology was employed to identify the most fitting combinations of hyperparameters for diverse machine learning models. The value of trial-and-error manifests through an iterative process that

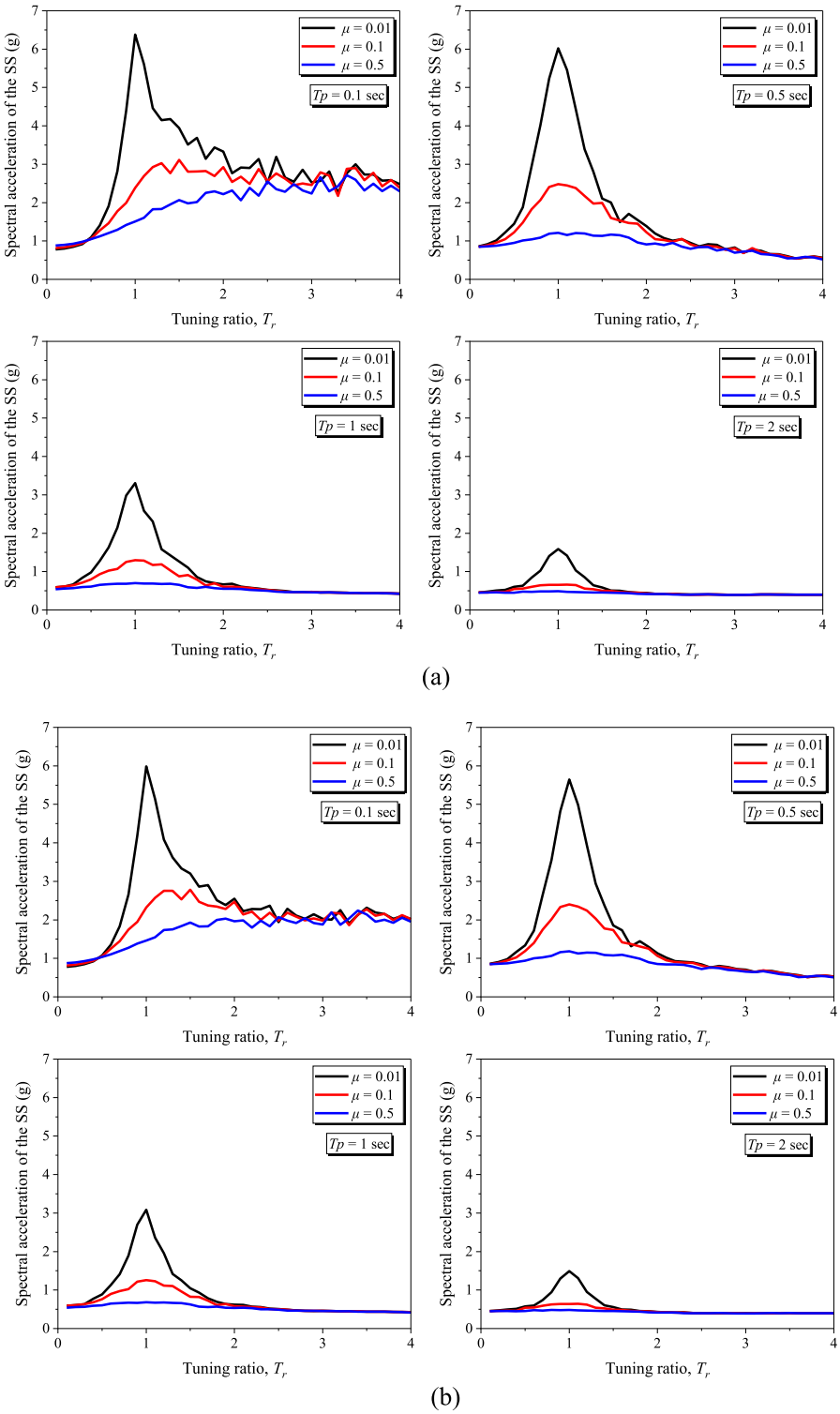

Fig. 5. Variation of floor response spectrum with tuning ratio for: (a) $\xi_s = 0.1\%$, (b) $\xi_s = 0.5\%$, (c) $\xi_s = 2\%$, and (d) $\xi_s = 10\%$.

progressively hones hyperparameters. The process commences with a basic set of hyperparameters, followed by meticulous monitoring of performance measurement outcomes, and eventual fine-tuning based on observations. This approach gains practicality, particularly when working with limited datasets, as advanced techniques like Bayesian optimization could be constrained by data availability. In such scenarios, trial and error emerges as a direct and efficient alternative. Analogous prediction challenges have led several researchers to opt for trial-and-error methodologies when developing ANN-based prediction models in their studies [24,42–44]. In our investigation, we comprehensively addressed all essential hyperparameters to optimize the model, with the exception of the learning rate. Notably, the Levenberg-Marquardt (LM) algorithm introduces a unique concept of the learning rate, distinct from conventional gradient descent-based

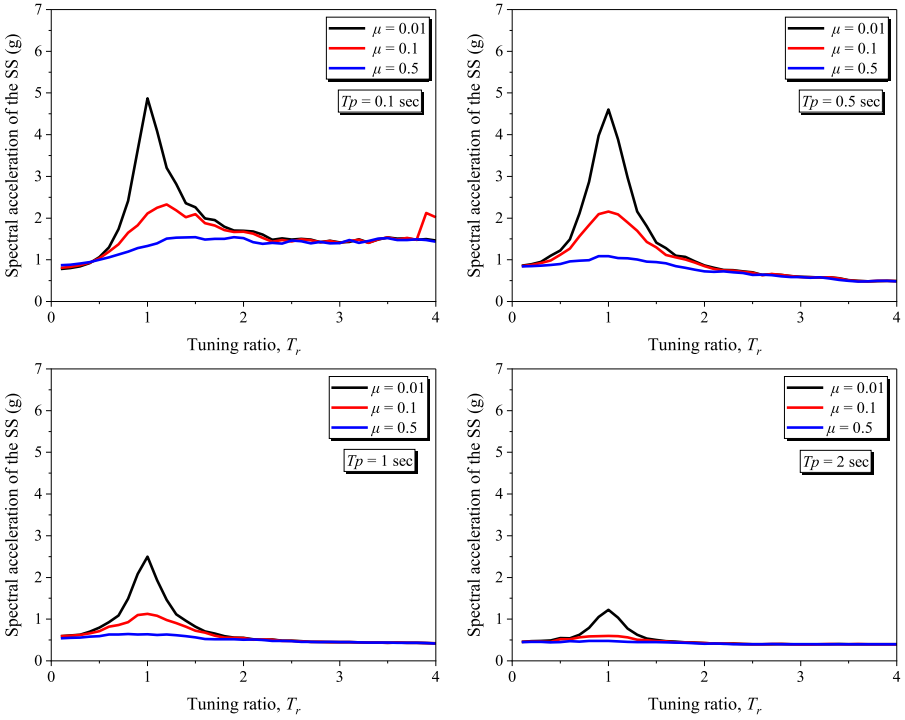

(c)

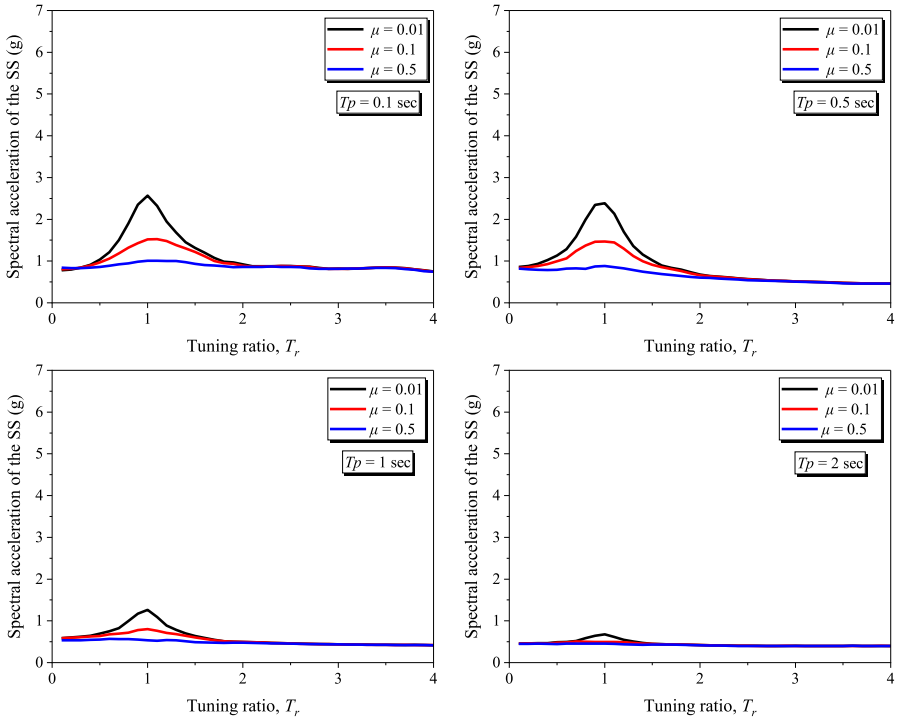

(d)

Fig. 5. (*continued*).

methods. Unlike the conventional fixed learning rate, the LM algorithm dynamically adjusts the step size using a damping factor, ensuring effective navigation of the error surface for achieving convergence.

The evaluation encompassed three specific types of neural networks: function fitting neural networks, feedforward neural networks, and cascade-forward neural networks. These networks incorporated an array of training and transfer functions, maintaining consistent transfer functions across hidden layers. The process was initiated by establishing the network and transfer functions. Multiple training functions or backpropagation algorithms were examined to determine the optimal choice. Subsequently, diverse transfer functions were explored based on the selected training function. This stepwise methodology ensured the selection of the most suitable combinations. The experimentation persisted by modifying the network function, repeating the process, and documenting the hyperparameter set that yielded the lowest mean absolute percentage error (*MAPE*), root mean squared error (*RMSE*), and

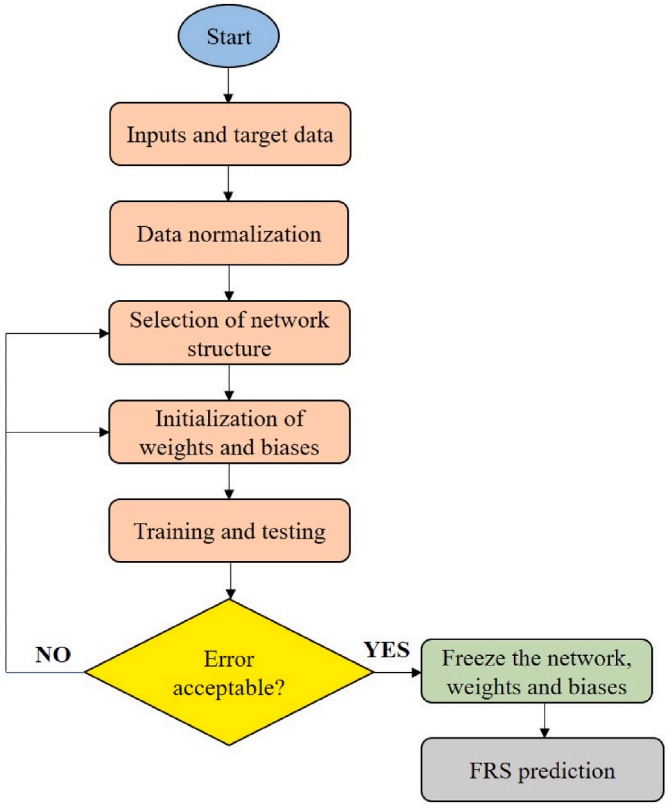

Fig. 6. Flowchart of presented procedure for predicting FRS.

Table 2
Statistical characteristics of the input dataset.

	T_r	T_p	ξ_s	μ
Count	39200	39200	39200	39200
Mean	2.05	1.05	2.685714	0.373
Standard deviation	1.154354	0.576635	3.376613	0.351775
Minimum	0.1	0.1	0.1	0.001
25%	1.075	0.575	0.2	0.01
50%	2.05	1.05	1	0.3
75%	3.025	1.525	5	0.7
Maximum	4	2	10	1

the highest coefficient of determination (R^2). The optimized hyper-parameter values are provided in Table 4. Hence, the present study attains accurate floor response spectrum (FRS) predictions through a two-layered feed-forward neural network. The network comprises an output layer and a hidden layer. In neural networks, achieving accurate function approximations is feasible with a single hidden layer [41]. Therefore, during the development of the ANN 4-10-1 model, the presence of 10 neurons in the hidden layer was considered (Fig. 7).

5.3. Development of the ANN-based prediction model

This section outlines the methodology to be adhered to for the construction of the predictive model. To train the hidden neurons, an appropriate learning technique must be created. The network is trained using the Levenberg-Marquardt (LM) variant of the backpropagation (BP) method. The Levenberg-Marquardt method, developed by Kenneth Levenberg and Donald Marquardt, provides numerical solutions for addressing nonlinear function problems. This neural network training technique is characterized by its speed and reliable convergence [45]. Transfer functions, alternatively termed activation functions and output functions, are the functions that govern the input-output relationship. The neural network model for this study utilized the Tan-sigmoid transfer function in output and hidden layers. MATLAB R2019b was employed as the environment for developing and training the network, offering the essential tools and capabilities. The dataset used in this study comprised a total of 39,200 floor spectral acceleration values.

Table 4
Optimal configuration of the ANN model.

Algorithm	Hyper-Parameter	Optimal Value
Artificial Neural Network (ANN)	Number of neurons in the input layer	4
	Number of hidden layers	1
	Number of output neuron	1
	Number of neurons in the hidden layer	10
	Training data	70%
	Testing data	15%
	Validation data	15%
	Number of epochs	1000
	Activation function	tanh
	Loss functions	*RMSE, MAPE*

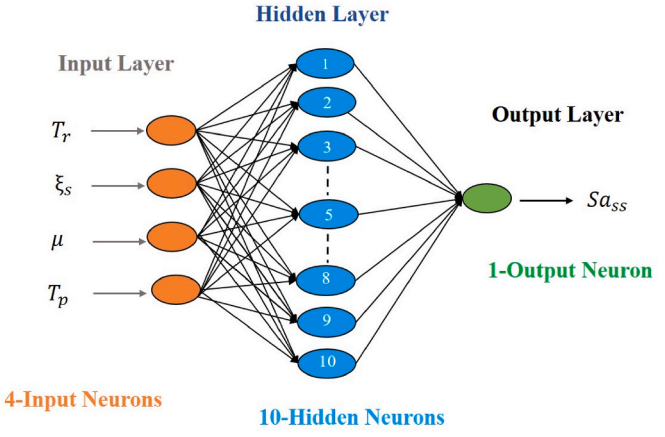

Fig. 7. ANN 4-10-1 model.

Table 3
Correlation matrix between different parameters.

	T_r	T_p	ξ_s	μ	Sa_{ss}
T_r	1	-3E-17	5.2E-17	1.8E-17	-0.2217
T_p	-3E-17	1	-8E-17	-1E-15	-0.4565
ξ_s	5.2E-17	-8E-17	1	9.8E-17	-0.1454
μ	1.8E-17	-1E-15	9.8E-17	1	-0.1949
Sa_{ss}	-0.2217	-0.4565	-0.1454	-0.1949	1

These values were simulated for 20 primary structural vibration periods (T_p), 40 tuning ratios (T_r), seven damping ratios of secondary structure (ξ_s), and seven mass ratios (μ). To ensure the proper training and evaluation of the neural network model, the dataset was divided into three subsets: a training set consisting of 70% of the entire data, a validation set comprising 15%, and a testing set containing the remaining 15%. Such division allows for robust training, validation, and assessment of the model's performance.

Before commencing the training process, the entire dataset underwent a preprocessing step. This involved normalizing the data to ensure that all variables were scaled to a range between −1.0 and 1.0. This normalization procedure grants equal importance to each variable during the analysis. The normalization process was achieved using Eq. (7).

$$X_n = \frac{2(X - X_{min})}{(X_{max} - X_{min})} - 1 \tag{7}$$

where X_n is the normalized value, X_{max}, X_{min} are the maximum and minimum values of the variable X. To evaluate the prediction capability of the ANN model, performance measurement functions are defined. The Root mean squared error (*RMSE*), mean absolute percentage error (*MAPE*), and coefficient of determination (R^2) are three such functions employed in this study. The performance functions (Eq. (8), (9), and (10)) are defined as follows:

$$RMSE = \sqrt{\frac{\sum (Y_s - Y_p)^2}{n}} \tag{8}$$

$$MAPE = \frac{\sum |Y_s - Y_p|}{\sum |Y_s - \overline{Y_s}|} \times \frac{100}{n} \tag{9}$$

$$R^2 = 1 - \frac{\sum (Y_s - Y_p)^2}{\sum (Y_s - \overline{Y_s})^2} \tag{10}$$

where, Y_s and Y_p are the simulated and predicted outputs, and n is the number of data points. Table 5 displays the outcomes of the model's performance. Fig. 8 displays the relationship between the predicted and simulated Sa_{ss}. The model provides accurate predictions of the Sa_{ss} values, as evidenced by the high correlation coefficient approaching unity.

5.4. Design expression using ANN

In this study, the ANN model with a configuration of 4 input neurons, 10 hidden neurons, and 1 output neuron, denoted as ANN-4-10-1, was employed to derive the mathematical equation for FRS. The connection weights obtained from the trained network can be utilized to formulate a mathematical equation by connecting the input and output parameters, as described in Eq. (11).

$$Y_n = f_o\left\{b_o + \sum_{k=1}^{h}\left[w_k * f_h\left(b_{hk} + \sum_{i=1}^{m} w_{ik}X_{ni}\right)\right]\right\} \tag{11}$$

where, b_o = bias of the output layer; w_k = weight connection between hidden layer neuron (k) and single output neuron; b_{hk} = kth hidden neuron bias; w_{ik} = weight between the input and hidden layer neuron (k); X_{ni} = input parameter; f_h = transfer function of the hidden layer (Tan-sigmoid); and f_o = transfer function of the output layer (Tan-sigmoid).

Upon substituting the values of weights and biases provided in Table 6 into Eq. (11), the predictive equation for the spectral acceleration of the SS (Sa_{ss}) was formulated. Eqs. 12–14 are then employed to obtain the normalized value of the spectral acceleration for the SS based on the input parameters.

$$a = (-0.088 * T_p) + (5.248 * T_r) + (5.611 * \mu) + (0.141 * \xi_s) + 8.998 \tag{12a}$$

$$b = (0.079 * T_p) - (5.377 * T_r) - (5.449 * \mu) - (0.140 * \xi_s) - 8.963 \tag{12b}$$

$$c = (0.176 * T_p) + (3.895 * T_r) - (0.165 * \mu) + (0.310 * \xi_s) + 3.174 \tag{12c}$$

$$d = (-0.028 * T_p) - (0.068 * T_r) + (0.453 * \mu) + (2.291 * \xi_s) + 5.059 \tag{12d}$$

$$e = (4.075 * T_p) + (7.311 * T_r) - (2.360 * \mu) + (0.239 * \xi_s) + 5.671 \tag{12e}$$

$$f = (-0.185 * T_p) - (20.95 * T_r) - (61.56 * \mu) - (0.515 * \xi_s) - 73.62 \tag{12f}$$

$$g = (2.337 * T_p) + (0.090 * T_r) + (0.001 * \mu) + (0.143 * \xi_s) + 3.702 \tag{12g}$$

$$h = (0.112 * T_p) + (0.243 * T_r) + (0.019 * \mu) + (0.014 * \xi_s) + 1.300 \tag{12h}$$

$$i = (-1.934 * T_p) + (0.030 * T_r) + (0.017 * \mu) - (0.145 * \xi_s) - 3.235 \tag{12i}$$

$$j = (-0.170 * T_p) - (20.97 * T_r) - (59.15 * \mu) - (0.489 * \xi_s) - 71.227 \tag{12j}$$

$$\begin{aligned} x = &-19.823 * tan\,h(a) - 19.660 * tan\,h(b) + 0.566 * tan\,h(c) - 16.848 \\ &* tan\,h(d) + 0.103 * tan\,h(e) + 15.007 * tan\,h(f) + 30.513 * tan\,h(g) \\ &- 17.395 * tan\,h(h) + 31.996 * tan\,h(i) - 15.298 * tan\,h(j) + 29.902 \end{aligned} \tag{13}$$

$$\text{Normalized } Sa_{ss}, (Sa_{ss})_{normalized} = tan\,h(x) \tag{14}$$

The Eq. (14) has been denormalized to obtain the Sa_{ss}. Eq. (15) yields the denormalized value of the required Sa_{ss}.

$$Sa_{ss} = 7.911 * \tanh(x) + 8.298 \tag{15}$$

Eq. (15) should be used only in the dataset range for which the neural network model was trained. Table 7 shows the maximum and minimum input and output parameter limitations.

Table 5
Performance of ANN model.

Dataset	R^2	*RMSE*	*MAPE*
Training	0.991	0.012	1.186
Testing	0.987	0.018	2.754

5.5. Validation of the ANN model

The main objective of this study was to assess the performance of a neural network model in accurately predicting the floor response spectrum, a critical parameter in the analysis and design of secondary structures. To ensure the ANN model's reliability, it was essential to validate its predictions against actual floor response spectra. Hence, in this section, an attempt has been made to compare the simulated spectra with ANN's predicted spectra for the damping ratios of 0.6% and 7%.

In the process of developing the neural network prediction model, the chosen damping ratio values for validation were deliberately excluded from the training dataset. This decision was made to test the model's ability to generalize and make accurate predictions on unseen instances, mimicking real-world scenarios where the model encounters new data points. The primary structural period is chosen as 0.5 s. The authors visually compared the simulated floor response spectra (constructed using the specified damping ratios) with the predicted spectra generated by the neural network model. The results were presented in

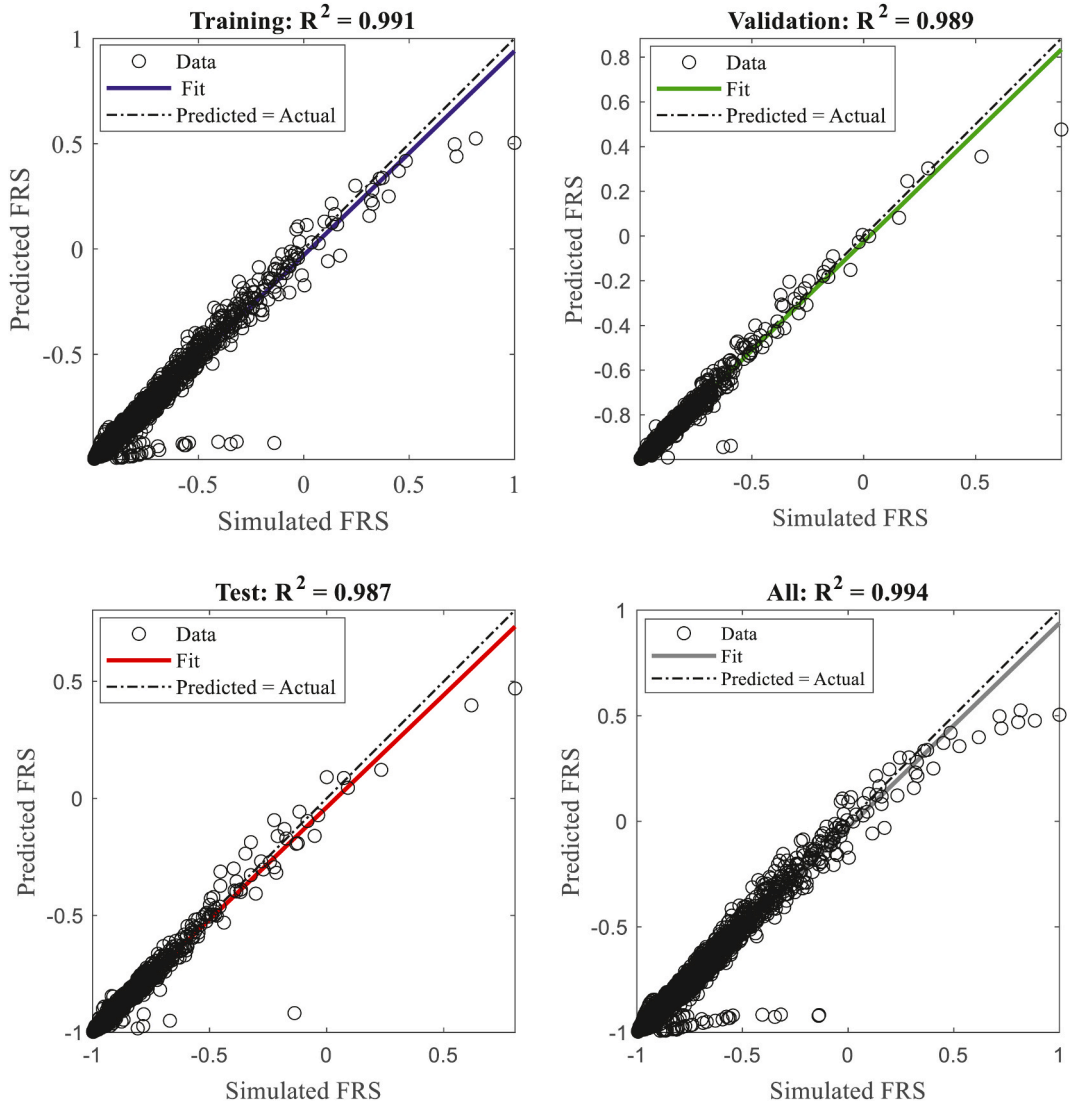

Fig. 8. Simulated and ANN's predicted FRS.

Table 6
Weights and biases of the 4-10-1 model.

Hidden Node	Input-Hidden weight				Hidden Output weight	Bias	
	T_p	T_r	μ	ξ_s	Sa_{ss}	Hidden	Output
1	−0.088	5.248	5.611	0.141	−19.823	8.998	29.902
2	0.079	−5.377	−5.449	−0.140	−19.660	−8.963	
3	0.176	3.895	−0.165	0.310	0.566	3.174	
4	−0.028	−0.068	0.453	2.291	−16.848	5.059	
5	4.075	7.311	−2.360	0.239	0.103	5.671	
6	−0.185	−20.955	−61.565	−0.515	15.007	−73.622	
7	2.337	0.090	0.001	0.143	30.513	3.702	
8	0.112	0.243	0.019	0.014	−17.395	1.300	
9	−1.934	0.030	0.017	−0.145	31.996	−3.235	
10	−0.170	−20.972	−59.153	−0.489	−15.298	−71.227	

Table 7
Limitations of input and output parameters.

	Input Parameters				Output Parameter
	T_s (sec)	T_r	μ	ξ_s (%)	Sa_{ss} (g)
Max	2	4	1	10	16.210
Min	0.1	0.1	0.001	0.1	0.3872

Fig. 9, which illustrated a comprehensive comparison between the two sets of spectra. Remarkably, the comparison demonstrated a significant level of agreement between the predicted and simulated floor response spectra across all investigated instances. This high level of agreement indicates the model's effectiveness in accurately capturing the complex relationships and patterns in the data, enabling it to make reliable predictions even for damping ratio values that were not explicitly part of the training process. The findings from this evaluation provide strong

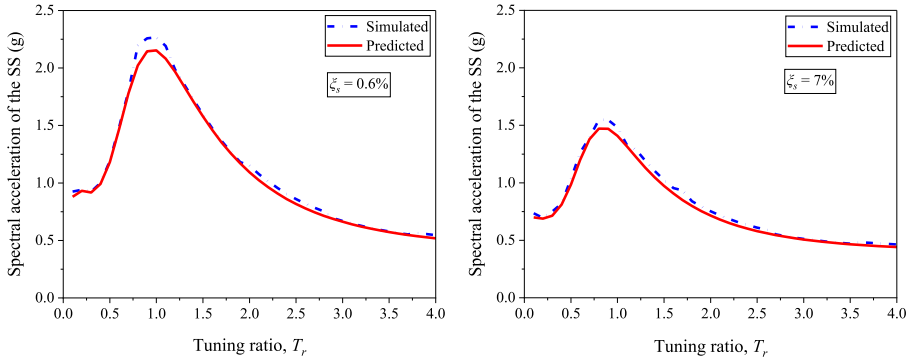

(a)

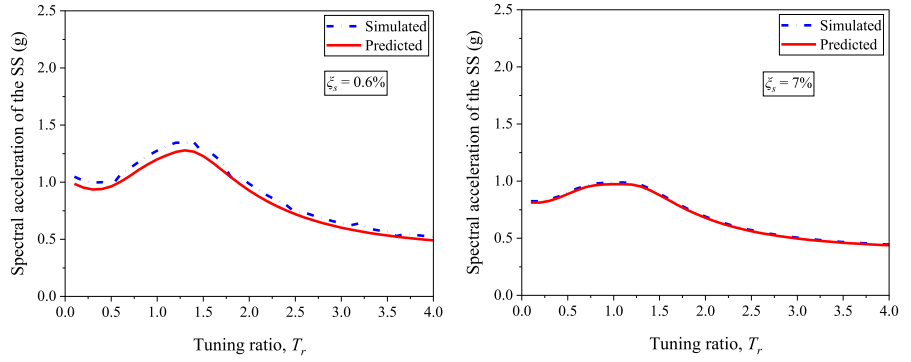

(b)

Fig. 9. Comparison between the simulated and predicted FRS for: (a) 0.1, (b) 0.5.

evidence of the neural network model's capability to generalize and accurately predict floor response spectra under different damping ratio conditions. This level of accuracy and agreement between the predicted and simulated spectra enhances the model's practical utility in real-world applications, where accurate floor response spectrum predictions are crucial for secondary structural analysis and design. The current study emphasizes simple systems exhibiting elastic dynamic behavior. However, the ANN model proposed herein holds promise for broader application by integrating non-linearity within primary and secondary structures during analysis. The authors intend to expand this investigation to encompass more intricate structures. As new data becomes accessible, the models can be further trained with updated datasets, enabling assessment of their suitability through real-world scenarios.

5.6. Comparing the predicted FRS with Eurocode 8 (EC8) formula

In this section, we have undertaken a comparison between the floor response spectra generated through the utilization of an Artificial Neural Network (ANN) model and the formulation outlined in Eurocode 8 [46]. According to EC8, the formulation for calculating the floor response spectrum acceleration, denoted as S_a, applied to a secondary structure is as follows:

$$S_a = \alpha.S.\left[\frac{3.\ (1+z/H)}{1+\left(1-T_s/T_p\right)^2}-0.5\right].g \geq \alpha.S.g \tag{16}$$

where α is the ratio between the ground and the gravity acceleration g, S is a soil amplification factor, z/H is the relative structural height at which the component is installed, T_s is the SS period, T_p is the fundamental period of the primary structure.

The design floor response spectrum is impacted by two main factors: the ratio between the period of the SS (T_s) and the natural period of the primary structural system (T_p), as well as the elevation at which the SS is installed within the primary structure. Eurocode's formulation offers a set of curves that depict the maximum values of spectral acceleration when T_s equals T_p for each floor. In Fig. 10 both elastic floor spectra and design Eurocode 8 floor spectra are plotted for the considered primary structure. When the mass from secondary structures (SSs) is minimal ($\mu = 0.001$), the Eurocode 8 (EC8) formulation tends to underestimate the maximum floor acceleration demand for SSs within the range of $0.8 \leq T_r \leq 1.2$. However, for comparable secondary structures with higher masses ($\mu = 0.1$ & 0.3), the EC8 formulation tends to overestimate the floor acceleration demand within the same T_r range. When the T_r is less than 0.5, the EC8 formulation consistently overestimates the acceleration demands on secondary structures (SS), regardless of the mass ratios. Conversely, when T_r exceeds 2.5, the EC8 formulation consistently underestimates the acceleration demands on secondary structures, again irrespective of mass ratios. Hence, it becomes evident that the EC8 formulation does not consider the dynamic interaction between the primary and secondary structures. Furthermore, it can be deduced that when the mass of the secondary structure is comparable to that of the primary structure within the range of $0.1 \leq T_r \leq 1.2$, the EC8 formulation for assessing demand on secondary structures tends to be excessively conservative. Fig. 10 illustrates a notable discrepancy wherein the definition outlined in EC8 significantly underestimates or overestimates the floor spectral acceleration. This discrepancy underscores the necessity to revise the existing code-based formulation. Incorporating the effects of dynamic interaction between the primary and secondary structures becomes imperative to enhance the accuracy of the formulation. This adjustment is crucial for better aligning the code-based predictions with observed spectral accelerations, thereby

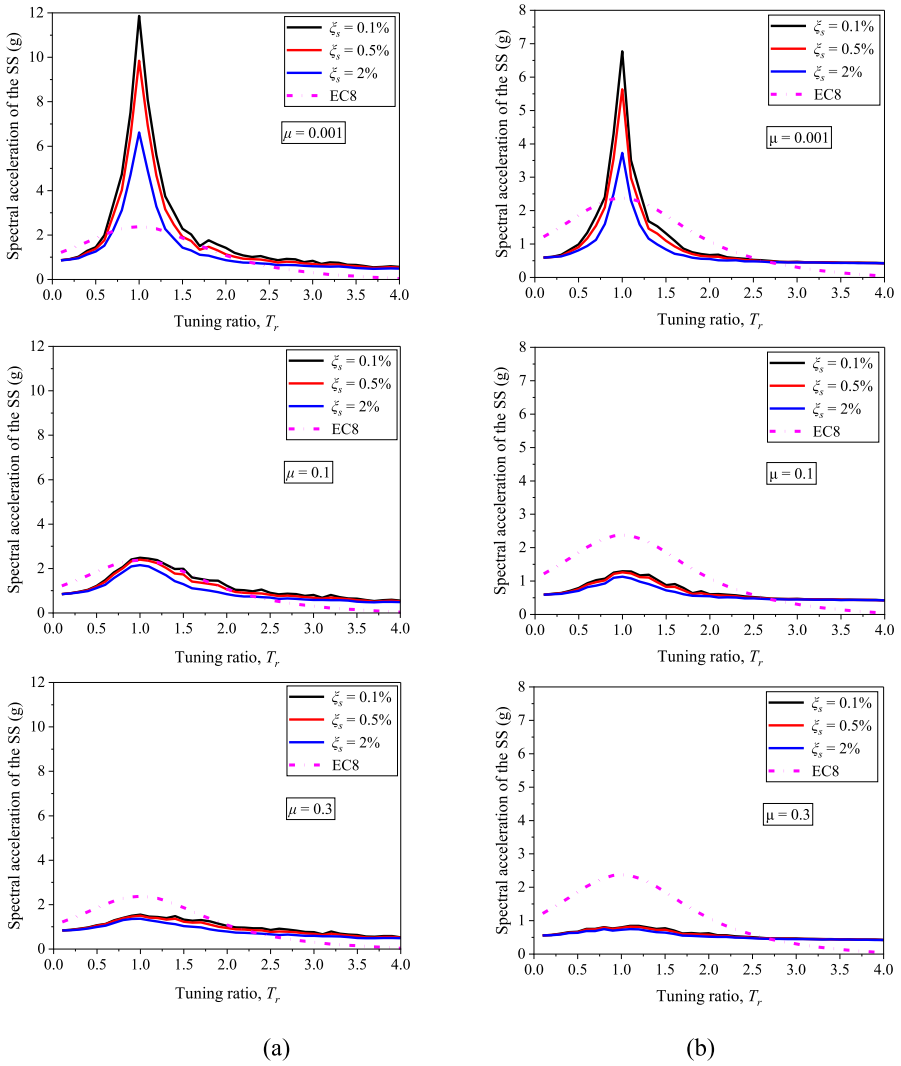

Fig. 10. Comparing predicted FRS with code-based FRS for (a) $T_p = 0.5$ s, (b) $T_p = 1$ s.

ensuring improved seismic performance evaluation and design considerations for secondary structures.

5.7. Sensitivity analysis

Sensitivity analysis is a vital aspect of Artificial Neural Network (ANN) modeling, as it offers valuable insights into the behavior and performance of the network. By assessing the impact of each input variable on the output, sensitivity analysis enables us to understand the relative importance of these variables. This knowledge is crucial for tasks like feature selection, where less influential variables can be discarded to enhance efficiency and interpretability. Another significant role of sensitivity analysis is in assessing the model's robustness. By systematically varying input values within predefined ranges, analysts can gauge how sensitive the ANN model is to changes. This evaluation is particularly valuable in applications where model accuracy and reliability are of utmost importance.

In this specific study, the researchers utilized Garson's algorithm [47] to investigate how different input variables influenced the floor response spectrum. Garson's algorithm, also known as Garson's method, is a technique designed to determine the importance of input variables in a neural network model. It offers a quick and intuitive way to estimate the relative contribution of each input variable to the network's output, without requiring complex computations or modifications to the network architecture. The algorithm works by dividing the connection weights between the input and hidden layers, as well as between the hidden and output layers, into partitions. These partitioned weights' absolute values are then used to calculate the input variables' relative importance, as outlined in Eq. (17). The partitioning of connection weights allows for the assessment of each input variable's contribution separately, based on the magnitude of the weights. Considering the absolute values of the partitioned weights enables the focus on their magnitudes rather than their positive or negative signs, which indicates the strength of the connections.

$$\text{Relative Importance } X_u = \sum_{j=1}^{n} \frac{\left|u_{w_{IH}^j}\right|}{\left(\sum_{k=1}^{N}\left|k_{w_{IH}^j}\right|\right)\left|w_{HO}^j\right|} \tag{17}$$

where,

X_u is the u^{th} input variable whose relative importance is to be determined
w_{IH} is the input-hidden neuron weight
w_{HO} is the hidden-output neuron weight,
n ($n = 10$) is the total number of neurons in the hidden layer
N ($N = 4$) is the total number of input variables

In Table 8, the weights shared among the nodes of the input and hidden layers in the neural network model can be seen. These weights correspond to the connections between the nodes of the input layer and the hidden layer. In contrast, Table 9 displays the weights between the nodes of the hidden layer and the output layer of the neural network model. These weights represent the connections between the nodes of the hidden layer and the single node in the output layer.

In Table 10, the relative importance and ranking of different input parameters are presented. The analysis of relative importance percentages and importance ranks provides valuable insights into how these input parameters affect the Floor Response Spectrum (FRS) in the neural network model. The results indicate that certain input parameters have a more substantial impact on the FRS than others. Specifically, the tuning ratio (T_r), T_p (vibration period of the primary structure), and the mass ratio (μ) of the secondary structure are identified as the most influential factors. This means that changes in these variables will significantly affect the behavior of the FRS. Therefore, it is crucial to carefully consider and accurately estimate these parameters when predicting or analyzing the FRS using the neural network model. On the other hand, the damping ratio (ξ_s) of the secondary structure is found to have a relatively lesser influence on the FRS. While it still contributes to the overall behavior, its impact is not as pronounced as the previously mentioned parameters. As a result, variations in the damping ratio may have a comparatively smaller effect on the FRS predictions for the considered case.

6. Summary and conclusions

The objective of this paper is to investigate the effect of a dynamic interaction on the seismic demands of a secondary structure. A detailed understanding of the primary-secondary-structure interaction is required for proper secondary structure design. Hence, a parametric study on the dynamic interaction of primary and secondary structures is discussed in this paper. The single-degree-of-freedom (SDOF) system is used for both the elastic primary structure (PS) and the elastic secondary structure (SS). The governing equations of motion for the coupled and uncoupled systems are developed and solved using the numerical method for a given set of ground motions. The dynamic interaction between the PS and SS shows an insignificant effect on the seismic behavior of the SS when the mass ratio is 0.001 (0.1%). Hence, at this mass ratio, the seismic demands on the secondary structure can be calculated using the uncoupled analysis. The dynamic interaction between the PS and SS shows a significant effect on the spectral acceleration response of the SS as the mass ratio increases. The coupled analysis is required only if the secondary structure is tuned to the vibration period of the primary structure, i.e., $0.8 \leq T_r \leq 1.2$. The uncoupled analysis is sufficient to analyze the seismic behavior of the secondary structure for $T_r < 0.5$ and $T_r > 2$. For a given damping ratio, the spectral acceleration of the secondary structure decreases with an increase in the vibration period of the primary structure, irrespective of the mass ratio.

In this research, Artificial Neural Networks (ANNs) were utilized to develop prediction models for the floor response spectrum. The inputs considered in the model are multiple factors, such as the tuning ratio (T_r), damping ratio (ξ_s), vibration period of the primary structure (T_p), and mass ratio (μ). These inputs play a significant role in determining the corresponding FRS, which serves as the ultimate output of the neural network model. The ANN model provides accurate predictions of the FRS values, as evidenced by the high correlation coefficient approaching unity. To verify the reliability of the ANN model, simulated spectra were compared with the model's predictions for two damping ratios: 0.6% and 7%. During the development of the neural network model, these specific damping ratio values were intentionally excluded from the training dataset and used for validation purposes. Furthermore, the sensitivity analysis conducted in the study shed light on the factors that significantly influence the FRS. The key parameters with considerable impact on FRS are the T_r, T_p, and μ. These variables play a crucial role in determining the behavior of FRS and should be carefully considered in any predictions or analyses related to it. Finally, ANN-based predicted spectra is compared against the spectra based on EC8 formulation. It can be deduced that when the mass of the secondary structure is comparable to that of the primary structure within the range of $0.1 \leq T_r \leq 1.2$, the EC8 formulation for assessing demand on secondary structures tends to be excessively conservative.

The findings of this study are confined to single-degree-of-freedom (SDOF) primary and secondary structures. Nevertheless, it's crucial to recognize that there are certain unaccounted factors that may exert substantial influence on structural responses. Notably, the study does not address the non-linear behavior of both primary and secondary structures. Furthermore, future research can broaden the scope by incorporating more intricate primary structures characterized by multiple degrees of freedom.

Funding

This research was funded by the Deanship of Scientific Research at King Khalid University, Saudi Arabia, grant number RGP.2/94/44. The authors extend their appreciation to the Deanship of Scientific Research at King Khalid University, Saudi Arabia, for funding this study as part of a large group project under grant number RGP.2/94/44.

CRediT authorship contribution statement

Madhavi Latha Annamdasu: Conceptualization, Data curation, Formal analysis, Investigation, Methodology, Software, Visualization, Writing – original draft. **S.P. Challagulla:** Conceptualization, Data curation, Formal analysis, Investigation, Methodology, Project administration, Resources, Software, Supervision, Validation, Visualization, Writing – original draft, Writing – review & editing. **Denise-Penelope N. Kontoni:** Conceptualization, Data curation, Formal analysis, Investigation, Methodology, Project administration, Resources, Software, Supervision, Visualization, Writing – review & editing. **J. Rex:** Resources, Validation. **Mohammed Jameel:** Funding acquisition, Software, Writing – review & editing. **Felipe Vicencio:** Formal analysis, Software.

Declaration of competing interest

The authors declare that they have no known competing financial interests or personal relationships that could have appeared to influence the work reported in this paper.

Table 8
Input and hidden neuron weights.

Input variable	w_{IH} (Input-hidden neuron weights)									
	N1	N2	N3	N4	N5	N6	N7	N8	N9	N10
T_P	−0.09	0.08	0.18	−0.03	4.07	−0.19	2.34	0.11	−1.93	−0.17
T_r	5.25	−5.38	3.90	−0.07	7.31	−20.95	0.09	0.24	0.03	−20.97
μ	5.61	−5.45	−0.16	0.45	−2.36	−61.57	0.00	0.02	0.02	−59.15
ξ_s	0.14	−0.14	0.31	2.29	0.24	−0.51	0.14	0.01	−0.15	−0.49

Table 9
Hidden and output neuron weights.

Output	w_{HO} (Hidden-output neuron weights)									
	N1	N2	N3	N4	N5	N6	N7	N8	N9	N10
FRS	−19.82	−19.66	0.566	−16.84	0.103	15.007	30.513	−17.39	31.996	−15.29

Table 10
Relative importance of input parameters.

Input variable	Outcome		
	Relative importance	Relative importance (%)	Rank
T_P	0.250	25.001	2
T_r	0.564	56.453	1
μ	0.156	15.666	3
ξ_s	0.028	2.880	4

Data availability

Data will be made available on request.

Acknowledgment

The authors wish to acknowledge the support of the Deanship of Scientific Research at King Khalid University, Saudi Arabia.

References

[1] Murty CVR, Goswami R, Vijayanarayanan AR, Kumar RP, Mehta VV. *Introduction to earthquake Protection of non-structural Elements in buildings*. Gujarat state disaster management authority. Government of Gujarat; 2012.
[2] Taghavi S, Miranda E. Estimation of seismic acceleration demands in building components. In: Proceedings of the 13th world conf. Earthq. Eng. Vancouver; 2004. p. 3199. B.C., Canada (1–6 August).
[3] Kamble V, Dayal Bharti S, Kumar Shrimali M, Kanti Datta T. Control of secondary systems response in a base-isolated building under tridirectional ground motion. Pract Period Struct Des Construct 2022;27:1–12. https://doi.org/10.1061/(asce)sc.1943-5576.0000641.
[4] Wang T, Shang Q, Li J. Seismic force demands on acceleration-sensitive nonstructural components: a state-of-the-art review. Earthq Eng Eng Vib 2021;20:39–62. https://doi.org/10.1007/s11803-021-2004-0.
[5] Sullivan TJ. Post-earthquake reparability of buildings: the role of non-structural elements. Struct Eng Int 2020;30:217–23. https://doi.org/10.1080/10168664.2020.1724525.
[6] Filiatrault A, Perrone D, Merino RJ, Calvi GM. Performance-based seismic design of nonstructural building elements. J Earthq Eng 2018;00:1–33. https://doi.org/10.1080/13632469.2018.1512910.
[7] Villaverde R. Fundamental concepts of earthquake engineering. CRC Press; 2009. 1439883114.
[8] Landge MV, Ingle RK. Comparative study of floor response spectra for regular and irregular buildings subjected to earthquake. Asian J. Civ. Eng. 2021;22:49–58. https://doi.org/10.1007/s42107-020-00297-1.
[9] Berto L, Bovo M, Rocca I, Saetta A, Savoia M. Seismic safety of valuable non-structural elements in RC buildings: floor response spectrum approaches. Eng Struct 2020;205:110081. https://doi.org/10.1016/j.engstruct.2019.110081.
[10] Surana M, Singh Y, Lang DH. Effect of irregular structural configuration on floor acceleration demand in hill-side buildings. Earthq Eng Struct Dynam 2018;47:2032–54. https://doi.org/10.1002/eqe.3054.
[11] Kelly JM, Sackman JL. Response spectra design methods for tuned equipment-structure systems. J Sound Vib 1978;59:171–9. https://doi.org/10.1016/0022-460X(78)90498-4.
[12] Lim E, Chouw N. Prediction of the response of secondary structures under dynamic loading considering primary–secondary structure interaction. Adv Struct Eng 2018;21:2143–53. https://doi.org/10.1177/1369433218768563.
[13] Salman K, Tran TT, Kim D. Grouping effect on the seismic response of cabinet facility considering primary-secondary structure interaction. Nucl Eng Technol 2019. https://doi.org/10.1016/j.net.2019.11.024.
[14] Smith-Pardo JP, Reyes JC, Ardila-Bothia L, Villamizar-Gonzalez JN, Ardila-Giraldo OA. Effect of live load on the seismic design of single-story storage structures under unidirectional horizontal ground motions. Eng Struct 2015;93:50–60. https://doi.org/10.1016/j.engstruct.2015.03.020.
[15] Sackman JL, Kelly JM. Seismic analysis of internal equipment and components in structures. Eng Struct 1979;1:179–90.
[16] Igusa T, Der Kiureghian A. Dynamic characterization of two-degree-of-freedom equipment-structure systems. J Eng Mech 1985;111:1–19.
[17] Singh MP, Suarez LE. Seismic response analysis of structure–equipment systems with non-classical damping effects. Earthq Eng Struct Dynam 1987;15:871–88. https://doi.org/10.1002/eqe.4290150708.
[18] Suarez LE, Singh MP. Floor response spectra with structure–equipment interaction effects by a mode synthesis approach. Earthq Eng Struct Dynam 1987;15:141–58.
[19] Challagulla SP, Suluguru AK, Noroozinejad Farsangi E, Manne M. Application of metaheuristic algorithms in prediction of earthquake peak ground acceleration. J Eng 2023;2023:e12269.
[20] Challagulla SP, Bhargav NC, Parimi C. Evaluation of damping modification factors for floor response spectra via machine learning model. Structures 2022;39:679–90.
[21] Challagulla SP, Parimi C, Anmala J. Prediction of spectral acceleration of a light structure with a flexible secondary system using artificial neural networks. Int J Struct Eng 2020;10:353–79.
[22] Bhargav NC, Challagulla SP, Farsangi EN. Prediction model for significant duration of strong motion in India. J Appl Sci Eng 2022;26:279–92.
[23] Yang T, Yuan X, Zhong J, Yuan W. Near-Fault pulse seismic ductility spectra for bridge columns based on machine learning. Soil Dynam Earthq Eng 2023;164:107582. https://doi.org/10.1016/j.soildyn.2022.107582.
[24] Payán-Serrano O, Bojórquez E, Bojórquez J, Chávez R, Reyes-Salazar A, Barraza M, López-Barraza A, Rodríguez-Lozoya H, Corona E. Prediction of maximum story drift of MDOF structures under simulated wind loads using artificial neural networks. Appl Sci 2017;7:563. https://doi.org/10.3390/app7060563.
[25] Blachowski B, Pnevmatikos N. Neural network based vibration control of seismically excited civil structures. Period Polytech Civ Eng 2018;62:620–8.
[26] Lima C, Martinelli E. Seismic response of acceleration-sensitive non-structural components in buildings. Buildings 2019;9:7. https://doi.org/10.3390/buildings9010007.
[27] Bagheri B, Nivedita KA, Firoozabad ES. Comparative damage assessment of irregular building based on static and dynamic analysis. Int J Civ Struct Eng 2013;3:505.
[28] Senaldi I, Magenes G, Penna A, Galasco A, Rota M. The effect of stiffened floor and roof diaphragms on the experimental seismic response of a full-scale unreinforced stone masonry building. J Earthq Eng 2014;18:407–43.
[29] Pnevmatikos NG, Thomos GC. Stochastic structural control under earthquake excitations. Struct Control Health Monit 2014;21:620–33.
[30] Peer PEER. Ground motion Database. *Pacific earthquake engineering research Centre (PEER). Berkeley, CA,* USA: University of California; 2023. https://peer.berkeley.edu/peer-strong-ground-motion-databases. ngawest2.berkeley.edu.
[31] ASCE 7-16. Minimum design loads and associated criteria for buildings and other structures (ASCE/SEI 7-16). Reston, Virginia: American Society of Civil Engineers (ASCE); 2016.
[32] NEHRP recommended seismic provisions for new buildings and other structures (FEMA P-750). National earthquake hazard reduction Program (NEHRP), building seismic safety council (BSSC) for the federal emergency management agency. Washington, DC, USA: FEMA); 2009.
[33] Khy K, Chintanapakdee C, Wijeyewickrema AC. Application of conditional mean spectrum in nonlinear response history analysis of tall buildings on soft soil. Eng J 2019;23:135–50. https://doi.org/10.4186/ej.2019.23.1.135.
[34] Alatik L, Abrahamson N. An improved method for nonstationary spectral matching. Earthq Spectra 2010;26:601–17. https://doi.org/10.1193/1.3459159.
[35] Haymes K, Sullivan TJ, Chandramohan R. A practice-oriented method for estimating elastic floor response spectra. Bull. New Zeal. Soc. Earthq. Eng. 2020;53:116–36. https://doi.org/10.5459/bnzsee.53.3.116-136.
[36] Adam C, Furtmüller T, Moschen L. Floor response spectra for moderately heavy nonstructural elements attached to ductile frame structures. In: Computational methods in earthquake engineering. Springer; 2013. p. 69–89.
[37] Surana M, Singh Y, Lang DH. Effect of structural characteristics on damping modification factors for floor response spectra in RC buildings. Eng Struct 2021;242:112514. https://doi.org/10.1016/j.engstruct.2021.112514.
[38] Jeng DS, Cha DH, Blumenstein M. Application of neural network in civil engineering problems. In: Proceedings of the international conference on advances in the internet, processing, systems and interdisciplinary research (IPSI 2003), sveti stefan, Montenegro; October, 2003. p. 4–11.
[39] Bhavani BD, Challagulla SP, Noroozinejad Farsangi E, Hossain I, Manne M. Enhancing seismic design of non-structural components implementing artificial intelligence approach: predicting component dynamic amplification factors. Int J Eng 2023;36:1211–8.
[40] Challagulla SP, Kontoni D-PN, Suluguru AK, Hossain I, Ramakrishna U, Jameel M. Assessing the seismic demands on non-structural components attached to reinforced concrete frames. Appl Sci 2023;13:1817. https://doi.org/10.3390/app13031817.
[41] Hornik K, Stinchcombe M, White H. Multilayer feedforward networks are universal approximators. Neural Network 1989;2:359–66.
[42] Sharma N, Dasgupta K, Dey A. Prediction of natural period of RC frame with shear wall supported on soil-pile foundation system using artificial neural network. J Earthq Eng 2020;00:1–25. https://doi.org/10.1080/13632469.2020.1824876.

[43] Ramezani M, Bathaei A, Ghorbani-Tanha AK. Application of artificial neural networks in optimal tuning of tuned mass dampers implemented in high-rise buildings subjected to wind load. Earthq Eng Eng Vib 2018;17:903–15. https://doi.org/10.1007/s11803-018-0483-4.
[44] Monjezi M, Hasanipanah M, Khandelwal M. Evaluation and prediction of blast-induced ground vibration at shur river dam, Iran, by artificial neural network. Neural Comput Appl 2013;22:1637–43.
[45] Hakim GPN, Hadi Habaebi M, Elsheikh EAA, Suliman FM, Islam MR, Yusoff SHB, Adesta EYT, Anzum R. Levenberg Marquardt artificial neural network model for self-organising networks implementation in wireless sensor network. IET Wirel Sens Syst 2023. https://doi.org/10.1049/wss2.12052.
[46] Eurocode 8. Eurocode 8: design of structures for earthquake resistance - Part 1 : general rules, seismic actions and rules for buildings (EN 1998-1). European Committee for Standardization (CEN), British Standards Institution; 2005.
[47] Garson GD. Interpreting neural-network connection weights. AI Expet 1991;6:46–51.